Inorganic Chemistry

Article

pubs.acs.org/IC

Synthesis and Structure of Perovskite $ScMnO_3$

Haiyan Chen,[†,#] Tian Yu,[†] Peng Gao,[†] Jianming Bai,[‡] Jing Tao,[§] Trevor A. Tyson,*[,†] Liping Wang,[∥,▽] and Roger Lalancette[⊥]

[†]Physics Department, New Jersey Institute of Technology, Newark, New Jersey 07102, United States

[‡]National Synchrotron Light Sources, Brookhaven National Laboratory, Upton, New York 11973, United States

[§]Condensed Matter Physics and Materials Science Department, Brookhaven National Laboratory, Upton, New York 11973, United States

[∥]Mineral Physics Institute, Stony Brook University, Stony Brook, New York 11794, United States

[⊥]Chemistry Department, Rutgers University, Newark, New Jersey 07102, United States

ABSTRACT: The rare-earth manganites $RMnO_3$ (R = rare earth) are a class of important multiferroics with stable hexagonal structures for small R ion radius (Sc, Lu, Yb, ...). Metastable perovskite phases of these systems possess intriguing electronically driven electrical polarization, but the synthesis of the perovskite phase for the end member $ScMnO_3$ system has proven to be elusive. We report the structure of a new monoclinic $P2_1/n$ perovskite phase of $ScMnO_3$ synthesized from the hexagonal phase under high-pressure and high-temperature conditions. This extends the small ion region for so-called E-phase electronically driven ferroelectric manganese perovsites.

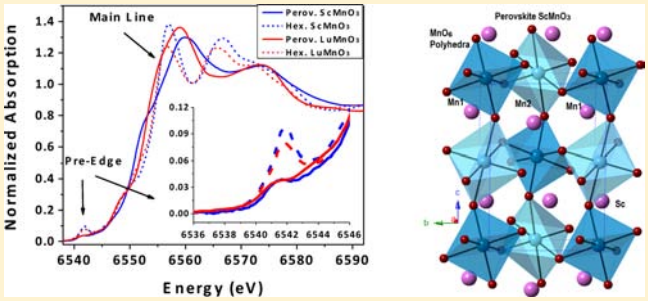

1. INTRODUCTION

Depending on the ionic radius of the rare-earth elements, $RMnO_3$ (R: rare-earth) manganites naturally form two types of structures: orthorhombic (R = La−Dy) and hexagonal (R = Sc, Y, Ho−Lu) structures.[1] Materials with both hexagonal and orthorhombic structures are found to exhibit simultaneous ferroelectric and magnetic properties, i.e., multiferroic behaviors, and these materials have potential in novel spintronic applications. Using high temperature and high pressure synthesis methods,[2] film deposition techniques,[3] and chemistry solution methods,[4] the hexagonal structure can be stabilized into the orthorhombic phase[5] for small ion sizes. Recently, orthorhombic perovskite materials with small ion sizes (such as $HoMnO_3$ and $LuMnO_3$) have become a topic of keen interest because of the possible existence of mainly electronically driven ferroelectricity (see refs 6, 8, and 9 and references therein). However, no detailed structural studies have been conducted on these systems assessing the relative weights of the charge and ion displacement components of ferroelectricity in these systems. Examining the full range of systems as a function of R ion size may lead to the discovery of an optimal system with high electric polarization.

For orthorhombic (O) $RMnO_3$ multiferroic materials with the perovskite crystal structure (space group *Pbnm*), the complex magnetic phase diagram[5,6] yields intriguing relationships between magnetic, dielectric properties and the lattice modulation with the ionic radius of *R*. With the small *R* ionic radius, the metastable O-$HoMnO_3$ does not show the incommensurate-commensurate transition, but is an E-type antiferromagnetic insulator. In the cases of $ErMnO_3$ and $YMnO_3$, they are found to be in the C-type magnetic phase below T_L.[7] For radii below that (starting at Ho), the metastable O-$RMnO_3$ systems are proposed to be E-type antiferromagnetic insulators. These systems have not been studied in detail experimentally and the origin of the predicted electric polarization is not understood.

Metastable O-$RMnO_3$ is difficult to prepare in a single crystalline form. Hence, the polycrystalline forms have mainly been examined. O-$HoMnO_3$ exhibits a dielectric constant which increases below T_N and a spontaneous polarization below T_L. Because of Ho^{3+} spin ordering at low temperature, the polarization shows strong magnetic field and temperature changes.[8] The large spontaneous polarization along the *a*-axis was suggested for E-type O-$RMnO_3$ in a combined model (atomic and electronic degrees of freedom) including the displacement mechanism and the spin−orbit coupling.[9]

The ionic radii for the R ions Y^{3+}, Ho^{3+}, Er^{3+}, Tm^{3+}, Yb^{3+}, Lu^{3+} and Sc^{3+} are 1.02, 1.02, 1.00, 0.99, 0.99, 0.92, and 0.87 Å, respectively.[10] For the perovskite system, R-site ion ranging from Y to Lu have a magnetic ordering temperature which is approximately constant ($T_N \approx 40$ K), while T_N for the corresponding hexagonal phase increases significantly with reduced ion.[2] The R site ion size indirectly changes the Mn−Mn interactions by modifying the Mn−O−Mn bond angles and distances. The significantly reduced size of the R radius for the

Received: July 1, 2013
Published: August 1, 2013

   dx.doi.org/10.1021/ic4016838 | *Inorg. Chem.* 2013, 52, 9692−9697

Table 1. Structural Parameters of Monoclinic $ScMnO_3$ from Single Crystal Refinement[a]

atom	x	y	z			
Mn1	0.5000	0.0000	0.0000			
Mn2	0.0000	0.5000	0.0000			
Sc	0.4760(2)	0.4289(3)	0.2688(2)			
O1	0.2963(9)	0.6836(9)	0.0954(6)			
O2	0.6493(10)	0.0746(9)	0.2278(6)			
O3	0.1820(10)	0.1898(9)	0.0530(6)			
Uij (Mn1)	0.0127(9)	0.0037(9)	0.0155(9)	−0.0020(5)	−0.0045(6)	0.0008(5)
Uij (Mn2)	0.0123(10)	0.0023(9)	0.0203(9)	−0.0012(6)	−0.0074(6)	0.0006(6)
Uij(Sc)	0.0123(8)	0.0029(8)	0.0196(8)	−0.0002(5)	−0.0025(5)	0.0007(5)
Uij(O1)	0.014(3)	0.005(2)	0.023(2)	0.003(2)	−0.007(2)	0.001(2)
Uij(O2)	0.018(3)	0.003(2)	0.022(3)	−0.000(2)	−0.005(2)	0.002(2)
Uij(O3)	0.016(3)	0.007(2)	0.027(3)	0.006(2)	0.001(2)	0.005(2)

space group: $P2_1/n$ (space group # 14)
a = 5.0534(3) Å, b = 5.3545(3) Å, c = 7.7572(4) Å
$\alpha = \gamma = 90.000°$, $\beta = 93.566(3)°$
D_x = 4.689 g/cm^3
measurement temperature: 293 K
crystal dimensions: 0.176 × 0.215 × 0.226 mm^3
wavelength: 1.54178 Å, $2\theta_{max}$: 140.93°
absorption coefficient: 74.49 mm^{-1}
EXTI extinction parameter: 0.00667(146)
$-5 \le h \le 5$, $-5 \le k \le 6$, $-9 \le l \le 8$
number of unique observed reflections $F_o > 4\sigma(F_o)$: 364
number of fitting parameters: 50
amplitude of peak/deepest hole in final difference map: 1.13 e/Å^3 (Sc1)
$R1$ = 4.09%, $R1 = (\Sigma||F_o| - |F_c||)/(\Sigma|F_o|)$
w$R2$ = 11.4%, w$R2 = [\Sigma w(F_o^2 - F_c^2)^2/(\Sigma w F_o^2)]^{1/2}$
goodness of fit = 1.146

[a]Atomic displacement parameters Uij are in the order: U_{11}, U_{22}, U_{33}, U_{23}, U_{13}, U_{12}.

$ScMnO_3$, the last member of this group, suggests that the perovskite phase of this system may possess interesting physics. Hence, we have attempted to stabilize this phase of $ScMnO_3$ to stimulate research, both experimentally and theoretically, into its properties by providing detailed information about its structure. Indeed, we have found a perovskite form of this material with structural characteristics similar to those of the Ho and Lu systems.

2. EXPERIMENTAL SECTION

Polycrystalline samples of hexagonal $ScMnO_3$ were prepared by solid-state reaction. Stoichiometric amounts of the starting materials, Sc_2O_3 (99.99%, GFS Chemicals) and MnO_2 (99.999%, Alfa Aesar) were ground and mixed well in an agate mortar and calcined in air at 1000 °C for 10 h. A second step of sample sintering was carried out in air at 1030 °C for 10 h and was repeated at 1100 and 1150 °C for 17 h with intermediate grindings. The resulting single phase powder sample was pressed into a pellet and annealed at 1100 °C for 10 h in O_2. Synthesis of monoclinic $ScMnO_3$ starting from hexagonal $ScMnO_3$ was carried out at the High Pressure Laboratory of the Mineral Physics Institute, Stony Brook University, using a 2000-ton split-sphere multianvil apparatus (USSA-2000). A 14/8 cell assembly was used, which consists of eight WC cubes (25 mm) with the 8 mm truncations as the second stage anvils, a ceramic MgO octahedron with an edge-length of 14 mm as pressure medium, a graphite sleeve as the resistive furnace, and a gold capsule as the sample container. The cell assembly with hexagonal $ScMnO_3$ inside was cold-compressed to target oil pressure and then heated. After annealing at 1100 °C and 12.5 GPa for 1 h, the sample was quenched to room temperature. Part of the synthesized pellet was then crushed and ground to a powder for further characterization by in situ synchrotron XRD, XAFS. For comparison, hexagonal and perovskite $LuMnO_3$ samples were prepared as given in ref 11. Electron diffraction experiments were carried out on a JEOL2100F transmission electron microscope (TEM) at the Center for Functional Nanomaterials, Brookhaven National Laboratory and TEM samples were crushed from bulk materials to be thin and electron transparent. All of the electron diffraction patterns were obtained from single-crystal domains and compared to simulations [Web Electron Microscopy Application Software (WebEMAPS)].[12]

Room temperature X-ray powder diffraction experiments on the $ScMnO_3$ sample were performed at beamline X14A of the NSLS and electron diffraction was performed at the Condensed Matter Physics and Materials Science Department, Brookhaven National Laboratory. The diffraction patterns were collected with a Si strip detector. For powder data collection, a rotating capillary was used and multiple patterns were averaged in a Q-range of 0.77 to 8.6 Å^{-1}. For in situ XRD experiments from room temperature to 1300 K, the powder sample was loaded in a sapphire tube (inner diameter = 0.7 mm) and heated by a custom-made microheater with a $MoSi_2$ heating element during spinning. The temperature was calibrated using CeO_2 as a standard and was controlled by computer via a Eurotherm 818 temperature controller. During warming, the XRD patterns were collected at constant temperature points. XRD pattern indexing was performed using software Jade 6.5 (Material Data, Inc.). Le Bail fitting of XRD profiles was accomplished using Jana 2006.[13] Preliminary structure solution from powder data was enabled by charge flipping algorithm using software Superflip[14] with reflection output from Jana 2006 and the final Rietveld structure refinement was performed using Jana 2006.

To refine the room temperature structure, high resolution room temperature single crystal structure was solved by selecting a single crystal grain of size 0.176 × 0.215 × 0.226 mm^3 from the powder sample. Single crystal X-ray diffraction measurements were conducted utilizing a Bruker APEX II diffractometer with 4K CCD detector and Cu K_α radiation (see details below in Table 1).

dx.doi.org/10.1021/ic4016838 | Inorg. Chem. 2013, 52, 9692−9697

X-ray absorption samples were prepared by brushing powder (500 mesh) onto Kapton tape and spectra were collected at beamline X19A, the National Synchrotron Light Source. A Mn foil reference was employed for energy calibration. The reduction of the X-ray absorption fine-structure (XAFS) data was performed using standard procedures.[15]

Heat capacity measurements of perovskite $ScMnO_3$ small single crystals in Apiezon H-Grease from 390 to 2 K were carried out with a Physical Property Measurement System (PPMS, Quantum Design). A small smooth contribution of the grease is present, but this does not alter the shape of the transition curve. For comparison, heat capacities of perovskite $HoMnO_3$ and $LuMnO_3$[16] are illustrated together.

3. RESULTS AND DISCUSSION

Figure 1(a) shows the near edge X-ray absorption spectra of both hexagonal (dashed lines) and perovskite (solid lines)

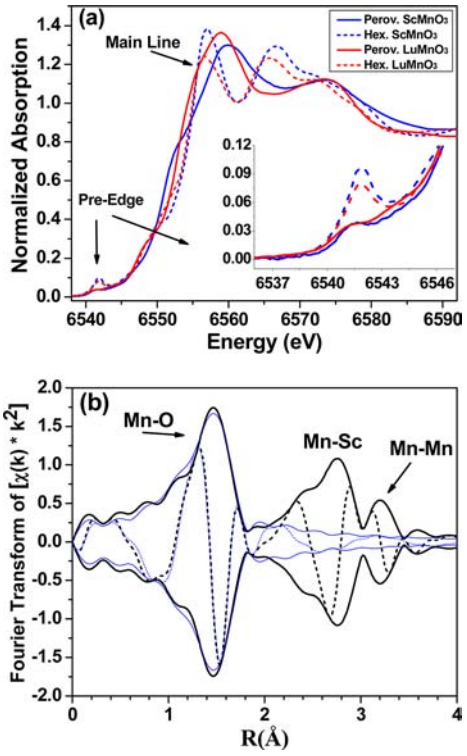

Figure 1. (a) Comparison of the Mn K-edge near-edge spectra of perovskite and hexagonal $ScMnO_3$ and $LuMnO_3$. (b) Fourier transform of the XAFS fine structure for the average Mn site of perovskite $ScMnO_3$. Blue lines (light) correspond to the model, while black (dark) lines correspond to the data. Dashed lines correspond to the imaginary part of the Fourier transform, while solid lines are for the amplitude envelope.

$RMnO_3$ systems for R = Sc and Lu. Focusing on the pre-edge in the inset, note that for the $LuMnO_3$ system there is a prominent feature near 6542 eV which is also duplicated in the hexagonal $ScMnO_3$ at the same position with larger amplitude. These features correspond to transitions to manganese 3d hybridized to oxygen 2p localized states, see ref 17 for perovskite case. The increase in the case of the Sc suggests enhanced d band localization. For the perovskite phase, again we see a feature near 6541 which is better resolved [localized hybridized Mn(3p)−O(2p)]. Note that the overall shape of the XANES spectra for the perovskite phases of both the Lu and Sc systems is the same indicating equivalent local structure and symmetry.

The Fourier transform of the full XAFS spectrum is shown in Figure 1(b). The first peak corresponds to the Mn−O nearest neighbor bonds and the higher peaks correspond to Mn−Sc and Mn−Mn (first neighbor), respectively. Additional information was gained by model fitting the first shell (Mn−O) of perovskite $ScMnO_3$ ([Figure 1(b)], solid line data and dashed line is model). The average Mn−O distance is found to be 2.028 Å (derived from a two shell XAFS fit yielding R1 = 1.910 ± 0.005 Å and N1 = 4; R2 = 2.27 ± 0.02 Å and N2 = 2 for data transformed over the range $2.78 < k < 13.2$ Å^{-1}) consistent with XRD results below (Table 1). More structural details can be gained from analysis of powder and single crystal X-ray diffraction data.

The powder XRD pattern of the high pressure high temperature synthesized sample is displayed in Figure 2

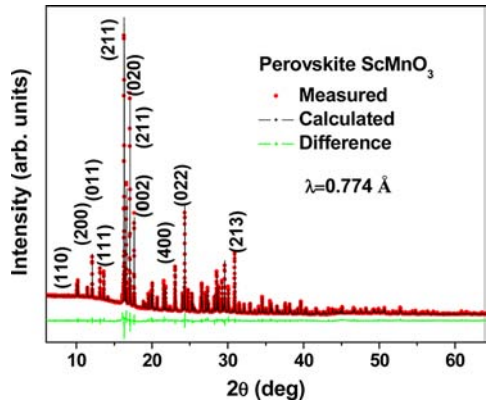

Figure 2. Powder XRD pattern of perovskite $ScMnO_3$ (black dotted line) and Rietveld refinement. The X-ray wavelength is 0.77376 Å and the Q range is 0.77 to 8.6 Å^{-1}.

(dotted line) compared to a preliminary model. This pattern was indexed to a monoclinic phase. Le Bail profile fitting yielded a fit with an R-factor $R_{wp} \approx 2.8\%$. Initial solution of the structure using the powder synchrotron XRD data was achieved using Superflip and subsequent Fourier difference maps. The positional and isotropic displacement parameters were refined. The refined profile with difference is displayed in Figure 2. A tentative space group of $P2_1$ was assigned based on the powder diffraction results (see below for final single crystal derived space group). The derived model was compared to the results of electron diffraction. In order to confirm the determined structure, electron diffraction patterns at zone axes [011], [111], [010] were obtained from the single-crystal domains of the compound and compared to simulations using the determined structure (Figure 3). The experimental patterns are found to be consistent with the simulations, strongly supporting the monoclinic determination of the crystalline structure.

To obtain an accurate crystal structure for this oxide, single crystal XRD measurements were performed. A full data set for a single crystal was collected at room temperature using Cu K_α radiation. The single crystal structure solution was conducted using SHELXL[18] after the data were corrected for absorption by face indexing.[19] Refinements revealed a monoclinic space group $P2_1/n$ with perovskite structure which is nonpolar analogous to $Pbnm$ for $LuMnO_3$[20] (nonpolar at room temperature). The full structural refinement results are given in Table 1, including the lattice parameters, atomic positions in the cell and the complete set of atomic displacement

dx.doi.org/10.1021/ic4016838 | Inorg. Chem. 2013, 52, 9692−9697

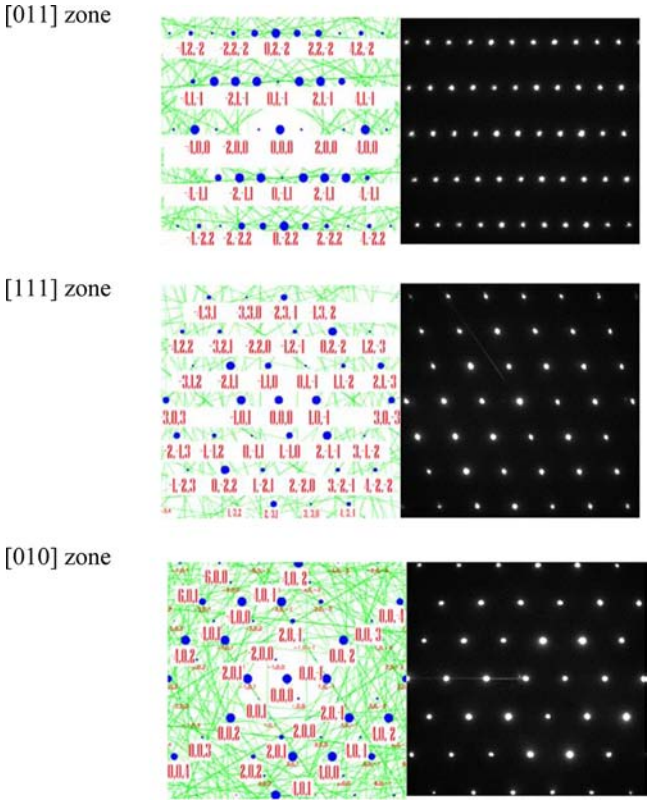

Figure 3. Electron diffraction patterns from single crystal domains of perovskite $ScMnO_3$ at zone axes [011], [111], and [010]. The left panels are the simulations using the provided structure and the right panels are the experimental patterns.

parameters (Uij) along with critical information on data used in the full refinement. Figure 4(a) shows the single crystal used in the measurement with some of the planes indexed, and in Figure 4(b) and 4(c) the perovskite structure for the Sc (middle) and Lu (bottom) systems are shown to indicate the similarity.

Selected bond lengths and bond angles are tabulated in Tables 2(a), 2(b), 3(a), and 3(b). Although the unit cell contains the same number of atoms, note that there are two distinct Mn sites (Mn1 and Mn2) in monoclinic $ScMnO_3$. Note that the average Mn−O distance is similar for both systems with Sc being just a little larger. However, the parameter $\varepsilon = -(1/N)\sum(R - \langle R\rangle)^2]^{1/2}$ which describes the distortion of the MnO_6 polyhedra is small for Mn1 and large for Mn2 with that for $LuMnO_3$ falling in between the value of both sites. The range of Mn−O bonds varies from ∼1.91 to ∼2.21 Å for $LuMnO_3$, while for Mn1 in $ScMnO_3$, we have ∼1.92 to ∼2.14 Å and for Mn2 we have ∼1.90 to ∼2.32 Å. Lu−O distances ranging from ∼2.19 to ∼2.55 Å, while the Sc−O distances cover the narrower and lower rage from 2.04 to 2.22 Å. The average Lu−O distance is ∼2.38 Å while that for Sc−O is ∼2.12 Å, which is significantly smaller. Hence, the spread in R−O distances is significantly smaller in Sc system than in the Lu system. These structural differences will impact the relative values of the electronic and structural components of the electric polarization.

Figure 5 shows the heat capacity of the perovskite $ScMnO_3$ compared to the same curves for the corresponding $LuMnO_3$ and $HoMnO_3$ systems (data for the latter two systems were taken from Tachibana et al., 2007). Note that the similar onset

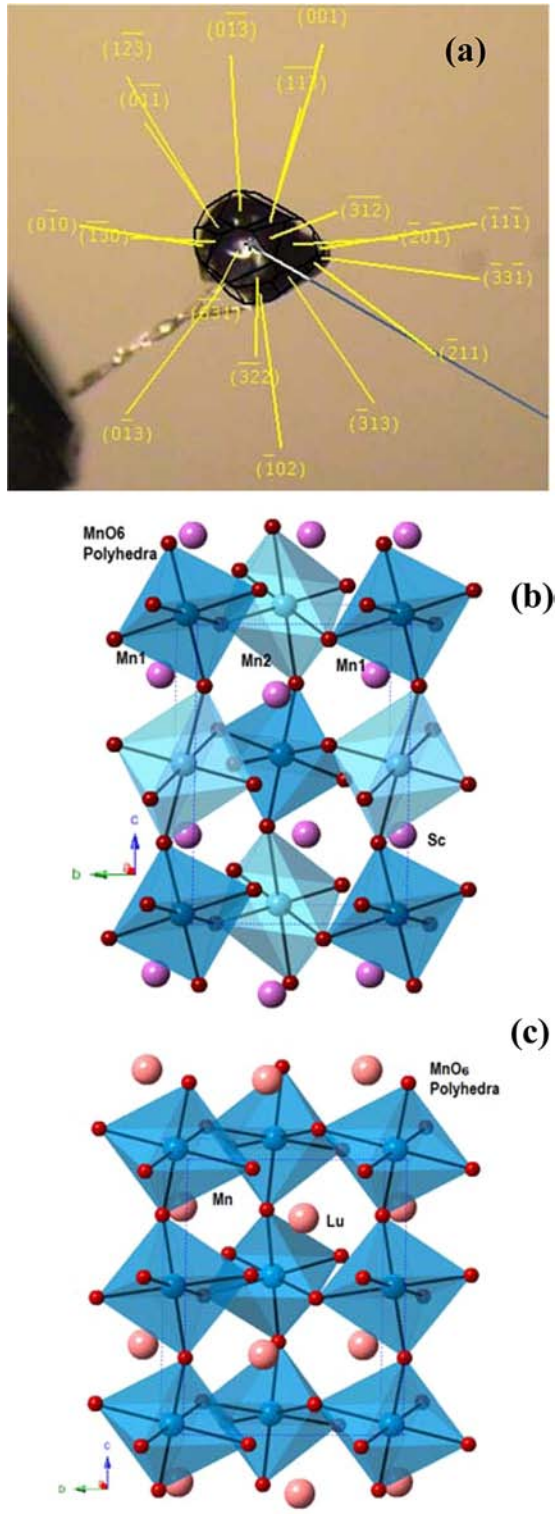

Figure 4. (a) A mounted $ScMnO_3$ single crystal for XRD measurements, (b) schematic views of the crystallographic structure of monoclinic $ScMnO_3$ (no-polar space group $P2_1/n$, left), and (c) orthorhombic $LuMnO_3$ (nonpolar space group *Pbnm*, right).

of the Neél temperature at low temperature in all cases with T_N increasing with reduced R ion size. The results indicate that perovskite $ScMnO_3$ has the highest T_N values reported to date and will stimulate research to enhance the magnetic ordering temperatures in E-phase perovskite systems.

dx.doi.org/10.1021/ic4016838 | *Inorg. Chem.* 2013, 52, 9692−9697

Table 2(a). Selected Bond Lengths of Monoclinic $ScMnO_3$ and Orthorhombic $LuMnO_3$

bond	bond length (Å)	bond	bond length (Å)
monoclinic $ScMnO_3$			
Mn1−O2 × 2	1.920(5)	Mn2−O1 × 2	1.902(5)
Mn1−O3 × 2	1.967(5)	Mn2−O3 × 2	1.930(5)
Mn1−O1 × 2	2.138(5)	Mn2−O2 × 2	2.320(5)
Mn1−Sc × 2	3.110(1)	Mn2−Sc × 2	2.912(1)
Mn1−Sc × 2	3.112(1)	Mn2−Sc × 2	3.108(5)
Mn1−Sc × 2	3.127(1)	Mn2−Sc × 2	3.492(5)
Mn1−Sc × 2	3.708(3)	Mn2−Sc × 2	3.543(2)
Sc−O1	2.084(5)	Sc−O1	2.215(2)
Sc−O2	2.047(5)	Sc−O3	2.153(2)
Sc−O2	2.122(5)	Sc−O3	2.462(5)
		Sc−O3	2.518(5)
orthorhombic $LuMnO_3$[a]			
Mn−O2 × 2	1.905(3)	Lu−O1	2.194(5)
Mn−O1 × 2	1.946(1)	Lu−O2 × 2	2.235(4)
Mn−O2 × 2	2.210(3)	Lu−O1	2.272(5)
Mn−Lu × 2	3.018(2)	Lu−O2 × 2	2.495(4)
Mn−Lu × 2	3.137(3)	Lu−O2 × 2	2.548(3)
Mn−Lu × 2	3.290(3)		

[a]Ref 20.

Table 2(b). Comparison of Averaged Bond Lengths of Monoclinic $ScMnO_3$ and Orthorhombic $LuMnO_3$

bond length	average (Å)	standard deviation (Å)	epsilon[a]
monoclinic $ScMnO_3$			
⟨Mn1−O⟩	2.0083	0.1027	0.0938
⟨Mn2−O⟩	2.0510	0.2089	0.1907
⟨Mn−O⟩	2.0297	0.1585	0.1518
⟨Mn−O⟩ XAFS	2.028	0.101	
⟨Sc−O⟩	2.1241	0.0648	0.0580
orthorhombic $LuMnO_3$[b]			
⟨Mn−O⟩	2.0202	0.1350	0.135
⟨Lu−O⟩	2.3776	0.1565	0.146

[a]The distortion parameter epsilon is defined as $\varepsilon = -(1/N)\sum(R - \langle R\rangle)^2]^{1/2}$, where N is the number of bonds, R is the bond distance, $\langle R\rangle$ is average bond distance (bonds < 3 Å). [b]Ref 20.

The structure as a function of temperature was explored by in situ high temperature synchrotron X-ray diffraction in air and analyzed by Le Bail fitting for temperature between room 300 and 1380 K (Figure 6). It is found that the perovskite phase is mostly converted into the more stable hexagonal phase of $P6_3cm$ symmetry on heating. After the heating cycle, the XRD pattern of the cooled sample was fit to a combination of hexagonal $P6_3cm$ and monoclinic perovskite $P2_1/n$ phases. The lattice parameter of the hexagonal phase component was found to be the same as the starting hexagonal $ScMnO_3$ used in the synthesis of this material.

4. CONCLUSIONS

Metastable perovskite-type phases of these systems possess intriguing electronically driven polarization, but the synthesis of the perovskite phase of the very small radius $ScMnO_3$ system has previously been proven to be difficult. Here we report a new small ion $ScMnO_3$ phase with perovskite-type structure synthesized from hexagonal $ScMnO_3$ under high-pressure and high-temperature conditions. A monoclinic $P2_1/n$ structure was

Table 3(a). Selected Bond Angles of Monoclinic $ScMnO_3$

$ScMnO_3$			
atoms	angle (°)	atoms	angle (°)
O2−Mn1−O2	180	O1−Sc−O1	115.87
O2−Mn1−O3 × 2	88.82(20)	O2−Sc−O2	87.28
O2−Mn1−O3 × 2	91.18(20)	O3−Sc−O3	75.28
O3−Mn1−O3	180.00(0)	O3−Sc−O3	121.98
O2−Mn1−O1 × 2	90.93(19)	O3−Sc−O3	131.55
O3−Mn1−O1 × 2	89.08(19)	O1−Sc−O2	97.13
O3−Mn1−O1 × 2	85.40(20)	O1−Sc−O2	145.25
O3−Mn1−O1 × 2	94.60(20)	O1−Sc−O2	130.99
O1−Mn2−O1	180	O1−Sc−O2	79.36
O1−Mn2−O3 × 2	89.50(21)	O1−Sc−O3	79.96
O1−Mn2−O3 × 2	90.50(21)	O1−Sc−O3	152.88
O1−Mn2−O2 × 2	81.35(19)	O1−Sc−O3	71.82
O1−Mn2−O2 × 2	98.65(19)	O1−Sc−O3	79.25
O3−Mn2−O2 × 2	82.42(19)	O1−Sc−O3	70.24
O3−Mn2−O2 × 2	97.58(19)	O1−Sc−O3	69.9
O2−Mn2−O2	180.00(32)	O2−Sc−O3	97.15
O3−Mn2−O3	180	O2−Sc−O3	75.4
Mn1−O1−Mn2	131.22(24)	O2−Sc−O3	135.17
Mn1−O2−Mn2	132.10(25)	O2−Sc−O3	148.12
Mn1−O3−Mn2	141.70(28)	O2−Sc−O3	75.39
		O2−Sc−O3	71.2

Table 3(b). Selected Bond Angles of Orthorhombic $LuMnO_3$[a]

$LuMnO_3$			
atoms	angle (°)	atoms	angle (°)
O1−Mn−O1 × 2	180.0(5)	O1−Lu−O1	91.16
O1−Mn−O2 × 2	85.20(14)	O1−Lu−O1	146.96
O1−Mn−O2 × 2	89.88(14)	O2−Lu−O2	78.13
O1−Mn−O2 × 2	90.12(14)	O2−Lu−O2	119.01
O1−Mn−O2 × 2	94.80(14)	O2−Lu−O2	76.91
O2−Mn−O2 × 2	88.76(11)	O2−Lu−O2	149.30
O2−Mn−O2 × 2	91.24(11)	O2−Lu−O2	75.63
O2−Mn−O2 × 2	180.0(5)	O2−Lu−O2	51.41
Mn−O1−Mn × 2	139.3(2)	O2−Lu−O2	98.12
Mn−O2−Mn × 4	141.85(15)	O1−Lu−O2	99.60
Mn−O1−Mn × 2	139.3(2)	O1−Lu−O2	138.92
Mn−O2−Mn × 4	141.85(15)	O1−Lu−O2	69.73
Mn−O1−Mn × 2	139.3(2)	O1−Lu−O2	49.63
Mn−O2−Mn × 4	141.85(15)	O1−Lu−O2	139.00
		O1−Lu−O2	56.40

[a]Ref 20.

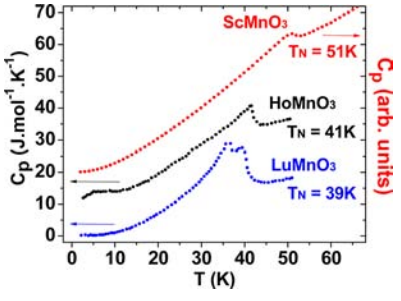

Figure 5. The specific heat curve of the monoclinic $ScMnO_3$ (solid circles, this work) compared to perovskite $HoMnO_3$ (star symbols) and perovskite $LuMnO_3$ (triangles) taken from Tachibana et al., 2007. The scans for Ho and Sc were offset successively by 10 J mol^{-1} K^{-1}.

dx.doi.org/10.1021/ic4016838 | Inorg. Chem. 2013, 52, 9692−9697

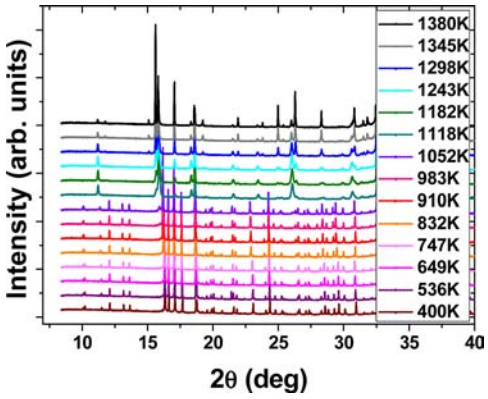

Figure 6. Stacked in situ XRD patterns of perovskite $ScMnO_3$ at different temperatures. The X-ray wavelength is 0.77485 Å. At high temperature, the perovskite phase is mostly converted back to the stable hexagonal phase. Note that the broad peak around $2\theta = 19°$ is from the sapphire tube and was accounted for during the Le Bail fitting.

found. Heat capacity measurements show an enhanced magnetic ordering temperature pointing to the possibility of function at higher temperatures for systems under pressure or strain. The monoclinic phase exhibits very similar structural parameters to the orthorhombic Ho and Lu systems and will stimulate experimental and theoretical investigations of the ground state magnetic order and possibly coupled electrical polarization and magnetism.

AUTHOR INFORMATION

Corresponding Author

*E-mail: tyson@njit.edu.

Present Addresses

[#]Mineral Physics Institute, Stony Brook University, Stony Brook, NY 11794.

[▽]HiPSEC and Department of Physics and Astronomy, University of Nevada, Las Vegas, Las Vegas, NV 89154.

Notes

The authors declare no competing financial interest.

ACKNOWLEDGMENTS

This work is supported by DOE Grant DE-FG02−07ER46402 (H.C., T.Y., P.G., T.A.T.). Synchrotron X-ray diffraction and X-ray absorption data acquisition were performed at Brookhaven National Laboratory's National Synchrotron Light Source (NSLS) which is funded by the U.S. Department of Energy. Single crystal X-ray diffraction measurements were performed at Rutgers University, Newark, NJ (NSF-CRIF Grant No. 0443538 (R.L.)). The Physical Properties Measurements System was acquired under NSF MRI Grant DMR-0923032 (ARRA award). TEM work performed was supported by the U.S. Department of Energy (Basic Energy Sciences) and by the Materials Science and Engineering Division under Contract No. DE-AC02−98CH10886 and through the use of the Center for Functional Nanomaterials at Brookhaven National Laboratory.

REFERENCES

(1) Prellier, W.; Singh, M. P.; Murugave, P. *J. Phys.: Condens. Matter.* **2005**, *30*, R803.

(2) Zhou, J. S.; Goodenough, J. B.; Gallardo-Amores, J. M.; Moran, E.; Alario-Franco, M. A.; Caudillo, R. *Phys. Rev. B* **2006**, *74*, 014422.

(3) Dubourdieu, C.; Huot, G.; Gelard, I.; Roussel, H.; Lebedev, O. I.; Tendeloo, G. van. *Philos. Mag. Lett.* **2007**, *87*, 203.

(4) Brinks, H. W.; Fjellvåg, H.; Kjekshus, A. *J. Solid State Chem.* **1997**, *129*, 334.

(5) Goto, T.; Kimura, T.; Lawes, G.; Ramirez, A. P.; Tokura, Y. *Phys. Rev. Lett.* **2004**, *92*, 257201.

(6) (a) Tsai, T. Y.; Lin, T. H.; Slowry, S.; Luo, C. W.; Wu, K. H.; Lin, J. Y.; Uen, T. M.; Juang, J. Y. *J. Phys.: Conf. Ser.* **2010**, *200*, 012210. (b) Barone, P.; Yamauchi, K.; Picozzi, S. *Phys. Rev. Lett.* **2011**, *106*, 077201. (c) Ren, C.-Y. *Phys. Rev. B* **2009**, *79*, 125113. (d) Picozzi, S.; Ederer, C. *J. Phys.: Condens. Matter.* **2009**, *21*, 303201. (e) Lin, T. H.; Hsieh, C. C.; Luo, C. W.; Lin, J. Y.; Sun, C. P.; Yang, H. D.; Hsu, C. H.; Chu, Y. H.; Wu, K. H.; Uen, T. M.; Juang, J. Y. *J. Appl. Phys.* **2009**, *106*, 103923. (f) Giovannetti, G.; Kumar, S.; Khomskii, D.; Picozzi, S.; Brink, J. v. d. *Phys. Rev. Lett.* **2009**, *103*, 156401. (g) Dong, S.; Yu, R.; Yunoki, S.; Liu, J. M.; Dagotto, E. *Eur. Phys. J. B* **2009**, *71*, 339−344. (h) Picozzi, S.; Yamauchi, K.; Sergienko, I. A.; Sen, C.; Sanyal, B.; Dagotto, E. *J. Phys.: Condens. Matter.* **2008**, *20*, 434208. (i) Dong, S.; Yu, R.; Yunoki, S.; Liu, J. M.; Dagotto, E. *Phys. Rev. B* **2008**, *78*, 155121. (j) Picozzi, S.; Yamauchi, K.; Sanyal, B.; Sergienko, I. A.; Dagotto, E. *Phys. Rev. Lett.* **2007**, *99*, 227201. (k) Picozzi, S.; Yamauchi, K.; Bihlmayer, G.; Blugel, S. *Phys. Rev. B* **2006**, *74*, 094402.

(7) Ye, F.; Lorenz, B.; Huang, Q.; Wang, Y. Q.; Sun, Y. Y.; Chu, C. W.; Fernandez-Baca, J. A.; Dai, P.; Mook, H. A. *Phys. Rev. B* **2007**, *76*, 060402.

(8) Lorenz, B.; Wang, Y.-Q.; Chu, C.-W. *Phys. Rev. B* **2007**, *76*, 104405.

(9) Sergienko, I. A.; Sen, C.; Dagotto, E. *Phys. Rev. Lett.* **2006**, *97* (22), 227204.

(10) Shannon, R. D. *Acta Crystallogr.* **1976**, *A32*, 751.

(11) Gao, P.; Chen, H. Y.; Tyson, A. T.; Liu, Z. X.; Bai, J. M.; Wang, L. P.; Choi, Y. J.; Cheong, S. W. *Appl. Phys. Lett.* **2010**, *97*, 262905.

(12) Web Electron Microscopy Application Software (WebEMAPS), http://emaps.mrl.uiuc.edu (accessed June 28, 2013).

(13) Petricek, V.; Dusek, M.; Palatinus, L. *Jana2006, The Crystallographic Computing System*; Institute of Physics: Praha, Czech Republic, 2006.

(14) Palatinus, L.; Chapuis, G. *J. Appl. Crystallogr.* **2007**, *40*, 786.

(15) (a) Konningsberger, D. C.; Prins, R. *J. Synchrotron Rad.* **2005**, *12*, 537. (b) *X-Ray Absorption: Principles, Applications, Techniques of EXAFS, SEXAFS and XANES*; Konningsberger, D. C., Prins, R., Eds.; Wiley: New York, 1988.

(16) Tachibana, M.; Shimoyama, T.; Kawaji, H.; Atake, T.; Takayama-Muromachi, E. *Phys. Rev. B* **2007**, *75*, 144425.

(17) Woo, H.; Tyson, T. A.; Croft, M.; Cheong, S.-W.; Woicik, J. C. *Phys. Rev. B* **2001**, *63*, 134412.

(18) (a) Muller, P.; Herbst-Irmer, R.; Spec, A. L.; Schneider, T. R.; Schneider, M. R. *Crystal Structure Refinement: A Crystallographer's Guide to SHELXL*; Oxford Press: Oxford, 2006. (b) Sheldrick, G. M. *SHELX-76: Program for Crystal Structure Determination*; Cambridge University: Cambridge, 1976.

(19) (a) Bruker (2008). *SADABS*; Bruker AXS Inc.: Madison, Wisconsin; (b) *SADABS: Area-Detector Absorption Correction*; Siemens Industrial Automation, Inc.: Madison, WI, 1996.

(20) Okamoto, H.; Imamura, N.; Hauback, B. C.; Karppinen, M.; Yamauchi, H.; Fjellvåg, H. *Solid State Comm.* **2008**, *146*, 152.